Hidden vorticity in binary Bose-Einstein condensates

Marijana Brtka,[1] Arnaldo Gammal,[2] and Boris A. Malomed[3]

[1]*Centro de Matemática, Computação e Cognição, Universidade Federal do ABC, 09210-170 Santo André, São Paulo (SP), Brazil*

[2]*Instituto de Física, Universidade de São Paulo, 05508-090 São Paulo, São Paulo, Brazil*

[3]*Department of Physical Electronics, School of Electrical Engineering, Faculty of Engineering, Tel Aviv University, Tel Aviv 69978, Israel*

(Received 16 June 2010; published 10 November 2010)

We consider a binary Bose-Einstein condensate (BEC) described by a system of two-dimensional (2D) Gross-Pitaevskii equations with the harmonic-oscillator trapping potential. The intraspecies interactions are attractive, while the interaction between the species may have either sign. The same model applies to the copropagation of bimodal beams in photonic-crystal fibers. We consider a family of trapped *hidden-vorticity* (HV) modes in the form of bound states of two components with opposite vorticities $S_{1,2} = \pm 1$, the total angular momentum being zero. A challenging problem is the stability of the HV modes. By means of a linear-stability analysis and direct simulations, stability domains are identified in a relevant parameter plane. In direct simulations, stable HV modes feature robustness against large perturbations, while unstable ones split into fragments whose number is identical to the azimuthal index of the fastest growing perturbation eigenmode. Conditions allowing for the creation of the HV modes in the experiment are discussed too. For comparison, a similar but simpler problem is studied in an analytical form, viz., the modulational instability of an HV state in a one-dimensional (1D) system with periodic boundary conditions (this system models a counterflow in a binary BEC mixture loaded into a toroidal trap or a bimodal optical beam coupled into a cylindrical shell). We demonstrate that the stabilization of the 1D HV modes is *impossible*, which stresses the significance of the stabilization of the HV modes in the 2D setting.

DOI: 10.1103/PhysRevA.82.053610 PACS number(s): 03.75.Lm, 42.65.Tg, 05.45.Yv, 42.70.Qs

I. INTRODUCTION

Vortices are fundamental topological excitations in Bose-Einstein condensates (BECs) [1]. In the case of repulsive interactions between atoms in a BEC, the vortices may be considered as two-dimensional (2D) dark solitons. Similar to their counterparts in self-defocusing optical media [2], the fundamental vortices with topological charge (spin) $S = 1$ are stable, while multiple vortices split into unitary ones. On the other hand, trapped BECs with attractive interactions may support *vortex solitons* (i.e., localized matter-wave modes with embedded vorticity). The creation of such solitons, which are subject to strong instabilities, remains a challenge to the experiment, although various stabilization schemes for them have been elaborated theoretically [3].

Vortex-soliton solutions are generated by the 2D Gross-Pitaevskii equation (GPE), which describes the BEC in the pancake geometry. Such a setting can be created using the superposition of a tight optical trap acting in the perpendicular direction (z), with confinement size a_z, and a loose harmonic-oscillator (HO) trapping potential with frequency Ω, induced by the nonuniform magnetic field in the (x,y) plane [4]. Accordingly, the underlying three-dimensional GPE may be reduced to its 2D counterpart under the condition that the HO length $a_{\rm ho} = \sqrt{\hbar/(m\Omega)}$ (m is the atomic mass) is much larger than a_z [i.e., $\Omega \ll \pi^2\hbar/(ma_z^2)$]. This condition is easy to realize in the experiment.

Vortex-soliton solutions that exist in the free 2D space [5] are unstable against the collapse. They are still more vulnerable to azimuthal perturbations, which break their axial symmetry, even if the collapse is suppressed by using a saturable or quadratic nonlinearity, instead of the cubic term [6] (full stabilization of vortex solitons in a part of their existence domain may be provided by competing nonlinearities, which include self-focusing and defocusing terms [7], or by nonlocal nonlinear terms [8], an example relevant to BECs being the stabilization of solitary vortices by the long-range dipole-dipole interactions [9]). In the 2D geometry, matter-wave solitons of the vortex type can be stabilized by an external potential periodic in x and y (optical lattice) [3,10], although such vortices completely lose their axial symmetry, being built as a set of four density peaks with phase shifts between them corresponding to topological charge $S = 1$. On the other hand, vortical states existing in the 2D linear Schrödinger equation with axisymmetric potentials (in particular, those represented by Bessel lattices) persist as stable states in the GPE with the *repulsive* nonlinearity [11].

The simplest 2D setting admitting stable solitons and vortices in the self-attractive BEC is based on the isotropic HO potential $m\Omega^2 r^2/2$, acting along radial coordinate r. The stability of trapped states in this setting was studied in several works [12,13]. In particular, zero-spin ($S = 0$) states are stable against the collapse, provided that their norm does not exceed the value corresponding to the collapse threshold in the free space (alias the norm of the *Townes soliton* [14]) $N < N_{\rm max}^{(S=0)}$. Formally, vorticity $S = 1$ gives rise to a dramatic increase of the 2D collapse threshold:

$$N_{\rm max}^{(S=1)} \approx 4N_{\rm max}^{(S=0)} \tag{1}$$

[5]. However, the actual increase of the stability limit for the vortex with $S = 1$ trapped in the HO potential is a more modest effect, amounting to $N_{\rm lim}^{(S=1)} \simeq (1/3)N_{\rm max}^{(S=1)}$. In an adjacent interval $0.33N_{\rm max}^{(S=1)} < N < 0.43N_{\rm max}^{(S=1)}$, the vortex exhibits a semistable behavior, periodically splitting into two fragments, which recombine back into the vortex. In the remaining part of the vortex's existence region $0.43N_{\rm max}^{(S=1)} < N < N_{\rm max}^{(S=1)}$, the fragments fail to recombine, undergoing collapse.

Another type of localized states, which seem to be vortices (axisymmetric modes with zero intensity at the pivot point), but carry zero net angular momentum, are known in several models of nonlinear optics involving two nonlinearly coupled-wave fields. These are *hidden-vorticity* (HV) modes, with two symmetric components carrying opposite spins, $S = \pm 1$. In particular, it was demonstrated that HV modes may be weakly unstable [15] or completely stable [16] in 2D bimodal systems with the saturable nonlinearity, including a model of photorefractive media [17]. The competition of cubic and quintic [18] or quadratic and cubic [19] self-focusing and self-defocusing terms may also stabilize spatial solitons of the HV type in the respective two-component systems. Stable HV modes were found in bimodal discrete systems too [20].

Systems of nonlinearly coupled GPEs are accurate models of binary BECs [21]. In this connection, a challenging problem is the stability of HV states in the binary condensate trapped in the HO potential. The difference from the above-mentioned systems studied in nonlinear optics is that, to the best of our knowledge, the stability of HV states has never been demonstrated in models with the (most fundamental) cubic nonlinearity. This is the subject of the present paper. We demonstrate that a finite-stability domain for such states can be found in the symmetric system, with the self-attraction acting in each component, while the interaction between the components may be both attractive and repulsive. The relative strength and *sign* of the self- and cross interactions in the binary BEC may be controlled by means of the Feshbach-resonance technique, which applies not only to single-component condensates, but also to their mixtures [22].

To better understand the purpose of the results produced by the system of coupled 2D GPEs, we also consider its one-dimensional (1D) version, with periodic (cyclic) boundary conditions (BC), which emulate the finite radius of the 2D HV modes trapped in the axisymmetric potential. Physical realizations of the 1D system subject to the cyclic BC are provided by a binary BEC mixture loaded into a toroidal trap, which is available to the experiment [23] or by a bimodal optical signal coupled into a hollow cylindrical waveguide. The 1D counterpart of the HV modes is represented by continuous waves (CWs) with equal amplitudes and opposite momenta of the components (i.e., counterflows in the two components of the binary BEC loaded into the toroidal trap). The similarity between the HV states in the 2D and 1D settings was mentioned in Ref. [16]; however, the role of the periodic BC was not considered there, and the nonlinearity was essentially different—saturable, rather than cubic. We demonstrate that the 1D HV modes can *never* be stabilized by the cyclic BC, which illustrates the nontrivial character of the stability of the HV modes in the 2D setting.

It is relevant to mention that objects called HVs were recently predicted in the single-component 2D BEC model including a rotating double-well potential [24]. These modes carry an explicit angular momentum, being hidden in the sense that their cores are not directly visible, sitting at the central barrier of the rotating potential. Another type of distantly related objects is ghost vortices that are located in a peripheral region of the single-component trapped BEC, which are almost invisible because of the vanishingly small density of the density supporting the ghosts [25].

The rest of the paper is structured as follows. The basic and auxiliary (2D and 1D) models and the necessary formalism are introduced in Sec. II. Stability domains for the symmetric HV modes in the 2D system are reported in Sec. III. In the same section, the development of instabilities accounted for by different modes of small perturbations are illustrated by direct simulations, for those 2D modes, which are unstable (the robustness of stable modes against strong random perturbations is illustrated too). The analytical investigation of the modulational (in)stability of the HV states in the 1D system with the periodic BC is briefly presented in Sec. IV. The paper is concluded in Sec. V.

II. THE MODEL AND TECHNICAL FRAMEWORK

A. The main (2D) and additional (1D) models

We start with the system of coupled GPEs in 2D, written for mean-field wave functions $\psi_{1,2}$ of the two components of the binary BEC. In the scaled form, the equations are [21]

$$i\frac{\partial \psi_1}{\partial t} = \left[-\frac{1}{2}\left(\frac{\partial^2}{\partial x^2}+\frac{\partial^2}{\partial y^2}\right)+\frac{1}{2}(x^2+y^2) - (|\psi_1|^2+\beta|\psi_2|^2)\right]\psi_1, \tag{2a}$$

$$i\frac{\partial \psi_2}{\partial t} = \left[-\frac{1}{2}\left(\frac{\partial^2}{\partial x^2}+\frac{\partial^2}{\partial y^2}\right)+\frac{1}{2}(x^2+y^2) - (|\psi_2|^2+\beta|\psi_1|^2)\right]\psi_2. \tag{2b}$$

We assume that the system is fully symmetric, with equal atomic masses and scattering lengths of the self-interaction in both components, as well as equal HO frequencies, which are rescaled to be 1. This setting implies that ψ_1 and ψ_2 represent two different hyperfine states of the same atomic species. Using the remaining scaling invariance, we set the coefficients of the self-attraction to be 1, while β, that may be both positive and negative, is the relative strength of the interaction between the species (attraction for $\beta > 0$ and repulsion for $\beta < 0$; as mentioned earlier, the sign of the intercomponent interaction may be reversed by means of the Feshbach-resonance technique). In the present notation, the collapse threshold for the symmetric ($\psi_1 = \psi_2$) zero-spin soliton is

$$N_{\max}^{(S=0)} \approx 5.85(1+\beta)^{-1} \tag{3}$$

[14] (recall this is the norm of one component, the total norm being twice as large; this expression makes sense for $\beta > -1$).

Equations (2), with t replaced by transmission distance z, apply as well to the description of the bimodal light propagation in photonic-crystal fibers [26], with fields $\psi_{1,2}$ representing two orthogonal linear polarizations of light. In that case, $\beta = 2/3$ is the most natural relative value of the *XPM* coefficient, but other values are possible too.

Equations (2) conserve two atomic numbers (norms of the components, or total powers of the two polarizations, in terms of the optical model) $N_{1,2} = \int\int |\psi_{1,2}(x,y,t)|^2\, dx\, dy$,

along with the energy (Hamiltonian) and the total angular momentum,

$$J = \int_0^{2\pi} d\theta \int_0^{\infty} r\, dr \left(\sum_{n=1,2} |\psi_n|^2 \frac{\partial \Phi_n}{\partial \theta} \right). \quad (4)$$

In Eq. (4), $\Phi_{1,2}$ are phases of complex wave functions $\psi_{1,2}$, and (r,θ) are the polar coordinates in the plane of (x,y) (obviously, angular momenta of each component are not conserved separately).

We seek for stationary solutions to Eqs. (2), for vortices with the HV, as

$$\psi_{1,2} = R_{1,2}(r) \exp(iS_{1,2}\theta - i\mu_{1,2}t), \quad S_1 = -S_2 = 1. \quad (5)$$

Note that total angular momentum (4) of such a state is simply related to the norms of its components: $J = S(N_1 - N_2)$, hence it vanishes for the states with equal norms, $N_1 = N_2$. In the following, we focus on the symmetric modes, with $R_1 = R_2 \equiv R$ and $\mu_1 = \mu_2 \equiv \mu$, where real function $R(x)$ obeys the equation,

$$R'' + r^{-1}R' + (2\mu - S^2 r^{-2} - r^2)R + 2(1+\beta)R^3 = 0. \quad (6)$$

In addition to the basic 2D model (2), we will consider the 1D system,

$$i\frac{\partial \psi_1}{\partial t} = \left[-\frac{1}{2}\frac{\partial^2}{\partial x^2} - \left(\frac{1}{|\beta|}|\psi_1|^2 + \mathrm{sgn}(\beta)|\psi_2|^2 \right) \right] \psi_1, \quad (7a)$$

$$i\frac{\partial \psi_2}{\partial t} = \left[-\frac{1}{2}\frac{\partial^2}{\partial x^2} - \left(\frac{1}{|\beta|}|\psi_2|^2 + \mathrm{sgn}(\beta)|\psi_1|^2 \right) \right] \psi_2, \quad (7b)$$

with the periodic BC,

$$\psi_{1,2}(x + 2\pi\varrho) \equiv \psi_{1,2}(x). \quad (8)$$

As mentioned previously, Eqs. (7) describe a binary BEC mixture confined in a toroidal trap of radius ϱ, or the copropagation of two optical waves in a cylindrical shell of the same radius. In these equations, the wave functions are rescaled, in comparison with Eqs. (2), by $\psi_{1,2} \to |\beta|^{-1/2}\psi_{1,2}$, the purpose of which is to include the limit case of $|\beta| \to \infty$. In the latter case, the nonlinearity is represented solely by the *XPM* term, implying that the intraspecies interaction may be effectively switched off by means of the Feshbach-resonance technique. The 1D system (7) conserves the two norms, $N_{1,2} = \int_0^{2\pi\varrho} |\psi_{1,2}(x,t)|^2\, dx$, Hamiltonian, and the total momentum, cf. Eq. (4):

$$P = \int_0^{2\pi\varrho} dx \sum_{n=1,2} \left(|\psi_n|^2 \frac{\partial \Phi_n}{\partial x} \right). \quad (9)$$

B. An outline of numerical methods

The stability of the stationary states was investigated by the linearization of the coupled GPEs for perturbed solutions, taken as

$$\psi_{1,2}(r,t) = [R(r) + u_{1,2}(r)e^{-i\omega t - iL\theta} + v_{1,2}^*(r)e^{i\omega^* t + iL\theta}]e^{-i\mu t + iS_{1,2}\theta}, \quad (10)$$

where integer L is the azimuthal index of perturbation eigenmodes with infinitesimal amplitudes $u_{1,2}(r)$, $v_{1,2}(r)$, and ω is the respective eigenvalue, the stability condition being $\mathrm{Im}\{\omega\} = 0$ for all the eigenvalues. The substitution of expression (10) into Eqs. (2) and the linearization lead to the following eigenvalue problem [cf. Ref. [27], that was dealing with the (in)stability of two-component modes with equal spins $S_1 = S_2$]:

$$\begin{pmatrix} D_1^- & -R^2 & -\beta R^2 & -\beta R^2 \\ R^2 & -D_1^+ & \beta R^2 & \beta R^2 \\ -\beta R^2 & -\beta R^2 & D_2^- & -R^2 \\ \beta R^2 & \beta R^2 & R^2 & -D_2^+ \end{pmatrix} U = \omega U, \quad (11)$$

where $U = (u_1, v_1, u_2, v_2)$, and the following set of operators is introduced: $D_m^{\pm} = -\Delta_r^{(L\pm S_m)}/2 + r^2/2 - (2+\beta)R^2 - \mu$, with $\Delta_r^{(M)} \equiv \partial^2/\partial r^2 + (1/r)(\partial/\partial r) - M^2/r^2$. Solutions $u_m(r)$ and $v_m(r)$ of Eq. (11) must exponentially decay at $r \to \infty$ and behave as $r^{|S_m \pm L|}$ at $r \to 0$.

Numerical solutions for stationary modes (5) were obtained by setting $\psi_{1,2} = R_{1,2}(r,t)\exp(iS_{1,2}\theta)$, and solving the corresponding radial reduction of Eqs. (2) in the imaginary time ($t \to -i\tau$, with real $\tau \geqslant 0$), following the lines of Ref. [28]. To this end, a grid formed by up to 400 points was used in interval $0 < r < 5$, and the integration in the imaginary time was run with step $\Delta\tau = 10^{-4}$. After producing stationary modes, the stability problem (11) was solved for azimuthal perturbation numbers $1 \leqslant L \leqslant 5$.

To check the predictions concerning the (in)stability of the HV states, direct numerical simulations of Eqs. (2) were run in real time, which added sufficiently strong random perturbations to the stationary modes. The real-time simulations were run by means of the D'yakonov [29] splitting algorithm and iterative solution of the nonlinear subsystem, with time step $\Delta t = 0.01$–0.001, and using up to 400×400 points in the Cartesian grid, which covered the domain $-10 < x, y < +10$.

III. NUMERICAL RESULTS FOR THE MAIN (2D) MODEL

A. The linear-stability analysis

Families of the stationary symmetric HV solutions are represented by curves $N(\mu)$ in Fig. 1, for several fixed values of coefficient $\beta > 0$, which account for the attraction between the species. As follows from Eq. (6), the curves that pertain to different values of β are actually equivalent to that for $\beta = 0$ because of the scaling invariance: $N(\mu,\beta) = N(\mu,0)/(1+\beta)$. In the limit of $N \to 0$, all the curves converge to $\mu = 2$, which is the eigenvalue of the linear Schrödinger equation for the isotropic HO potential [i.e., Eq. (6) with the last term dropped], which corresponds to $S = 1$. As for shapes of the HV modes, they can be seen as initial images displayed later in Figs. 6–9.

The most essential issue is the stability of the HV modes. The respective findings, produced by the systematic numerical solution of the eigenvalue problem (11), are collected in Fig. 2. In this figure, the instability growth rates, $\gamma_L \equiv |\mathrm{Im}\{\omega_L\}|$, are displayed as functions of the HV-mode's chemical potential, for perturbation azimuthal numbers $L = 1,2,3,4$ and several values of the nonlinear-coupling coefficient β (no instability was found for $L \geqslant 5$). Each panel reveals *instability-free windows*, which abut on the edge point, $\mu = 2$ (i.e., $N = 0$).

In particular, a large stability region $1.09 \leqslant \mu \leqslant 2$, which corresponds to $N \leqslant 7.76$, exists for $\beta = 0.2$. In this case,

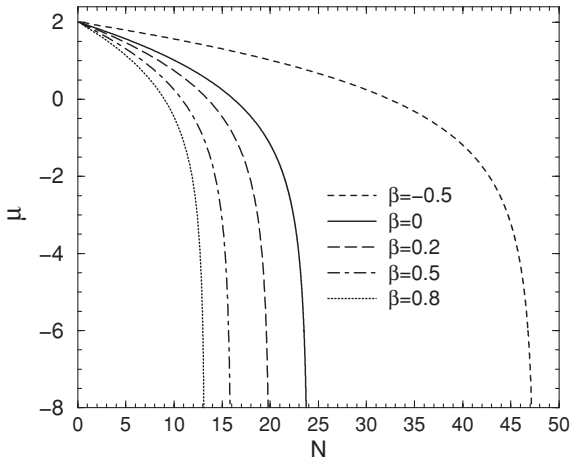

FIG. 1. Chemical potential μ of the HV symmetric modes versus norm N (of one component), for different values of interaction parameter β.

the instability at $\mu < 1.09$ is dominated by the perturbation mode with $L = 2$. An interesting situation is observed for $\beta = 0.235$: As seen in the inset to the respective panel in Fig. 2, the stability region is split into two parts by an interval of a very weak instability (in the physical applications, such a weak instability may be ignored). In other cases displayed in Fig. 2, $\beta = \pm 0.5$, different perturbation azimuthal numbers L play the dominant role in different parts of the instability regions.

The overall results are further summarized in the form of the stability diagram displayed in Fig. 3, which depicts both the stability domain, in the plane of (N,β), and those regions where perturbation eigenmodes, which pertain to $L = 1$, 2, 3, or 4, control the instability. According to Eqs. (1) and (3), the border of the forbidden region, in which the HV modes do not exist, is located at $N = N_{\max}^{(S=1)} \approx 23.4(1+\beta)^{-1}$. The cut of the stability diagram through $\beta = 0$ is tantamount to findings reported for the single-component model in Ref. [13] (in particular, the relative width of the stability domain, with respect to the existence region, is $\simeq 1/3$, as mentioned before).

Naturally, the stability domain is larger at $\beta < 0$, as the repulsion between the components helps to stabilize the HV mode. The stability domain abruptly shrinks with the increase of $|\beta|$. In fact, at large $|\beta|$, only the quasilinear HV mode, which corresponds to very small N, remains stable, which is explained by the fact that the vortex eigenstates in the isotropic HO potential are stable within the framework of the linear Schrödinger equation. It is also worthy to note that the instability regions dominated by the perturbation modes

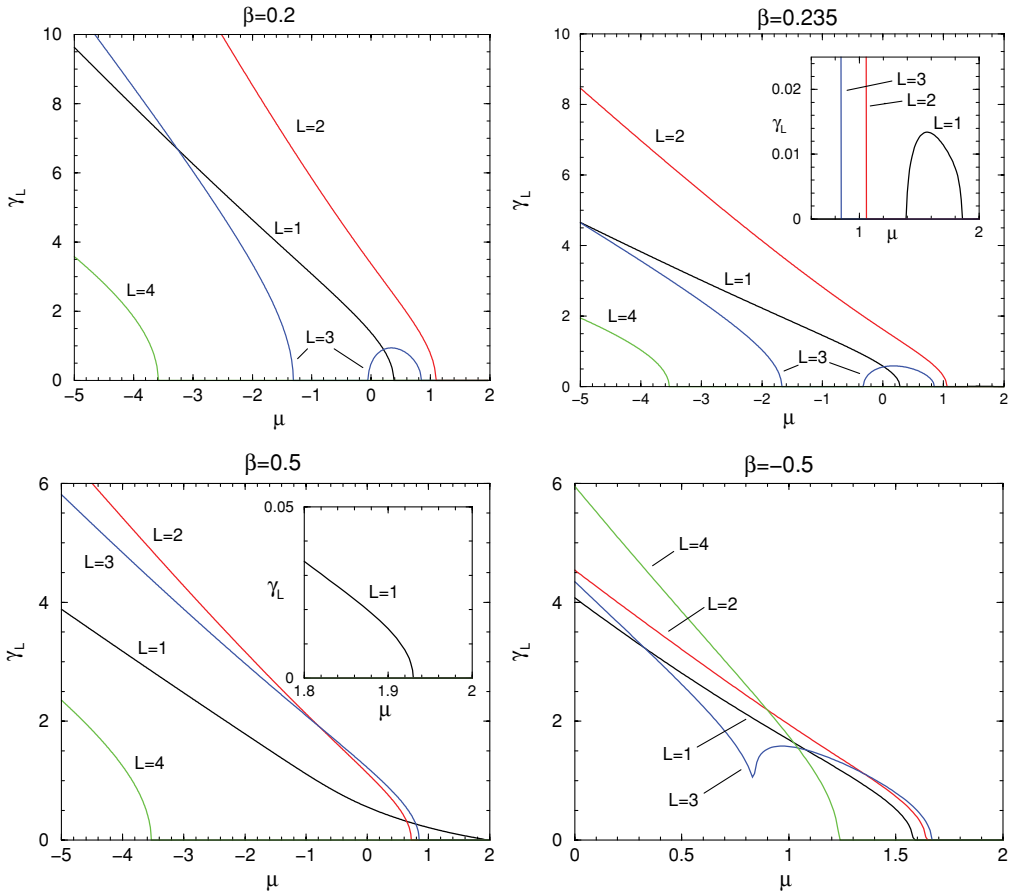

FIG. 2. (Color online) The instability growth rates for different values of the azimuthal index (L) of the perturbation eigenmodes, and different fixed values of the interaction coefficient β. Insets display blowups of portions of the diagrams which are critical to the identification of the stability regions.

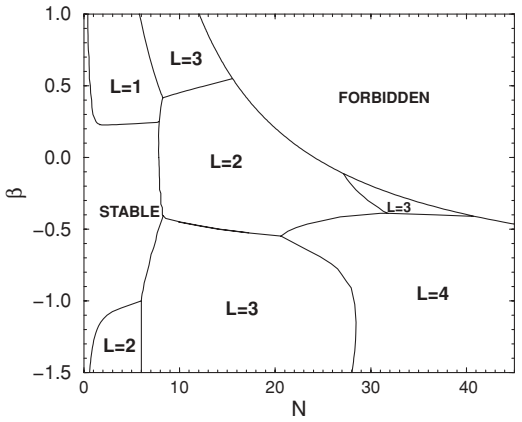

FIG. 3. The stability diagram for symmetric HV modes, in the plane of the norm (of one component) and interaction coefficient. Instability areas are labeled by the azimuthal index of the dominating perturbation eigenmode.

with $L = 2$, 3, and 4 are split, respectively, into two, three, and four disjoint segments.

The predicted stable HV states can easily be interpreted in terms if experimental parameters—in particular, for different hyperfine states in ^{7}Li (in fact, the estimates are not essentially different from those pertaining to stable vortices trapped in the single-component BEC [13]). Rewriting the underlying equations (2) in physical units, with the HO trapping frequency $\omega = 2\pi \times 10$ Hz and the scattering length of the interatomic interactions $a_s \simeq -0.1$ nm, we conclude that the largest number of atoms in the stable HV states, corresponding to scaled norm $N \lesssim 10$ in Fig. 3, is estimated as 10^5, while the characteristic radius of the HV ring-shaped pattern is 10 μm, and the time unit in the scaled notation corresponds to $\sim$0.1 ms.

B. Direct tests of the stability and self-trapping

The predictions of the linear-stability analysis have been checked by means of direct simulations. First, systematic simulations, using large random perturbations added to the HV modes, demonstrate that all the modes which were predicted to be stable are indeed robust objects, which keep their intrinsic HV structure (vorticities $S = \pm 1$ of the two components) and quickly relax to the unperturbed shape through an effective self-cleaning. We stress that the perturbations had a random structure in the plane of (x, y), hence they tested the stability of the HV states against both the collapse and the breakup of the axial symmetry. A typical example is displayed in Fig. 4. Note that, although the HV mode, the stability of which is tested in the figure, is located close to the upper and right borders of the stability area in Fig. 3 (at $N = 7.05$ and $\beta = 0.2$) and the random amplitude perturbation is large enough (5%), the HV pattern exhibits a very fast self-cleaning and suppression of the perturbation. By the moment of time $t = 0.1$, the perturbation remains only in small ripples of the phase pattern, which safely keeps the initial vorticity.

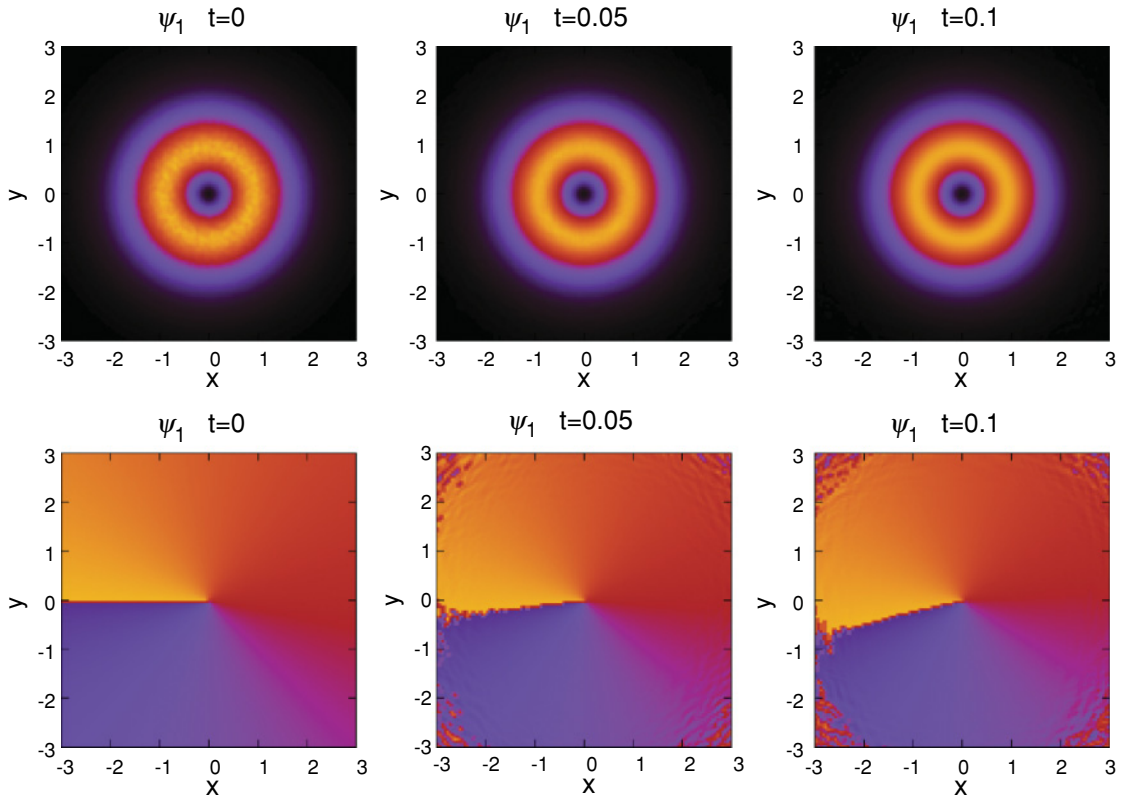

FIG. 4. (Color online) The top and bottom panels display, respectively, the evolution of the density and phase of the first component (ψ_1) of a perturbed stable HV mode with half-norm $N = 7.05$ and $\mu = 1.2$, at $\beta = 0.2$. The initial state (at $t = 0$) includes a random perturbation of $|\psi_1(x, y)|$ at the 5% level. The self-cleaning of the perturbed mode was practically completed by $t = 0.1$.

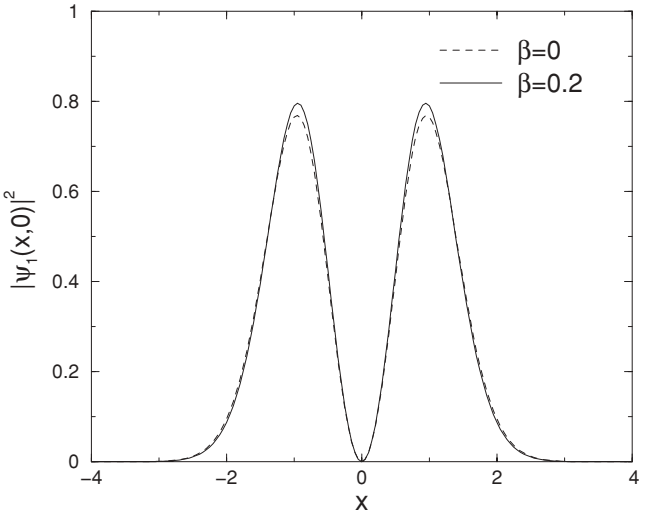

FIG. 5. The density-profile cross sections drawn through the center [i.e., $|\psi_1(x,0)|^2$] for the initial single-component vortical state, which corresponds to $\beta = 0$, and for the eventual self-trapped HV mode, which pertains to $\beta = 0.2$. The norm of the mode (in one component) is $N = 5.65$, and the chemical potential of the initial single-component vortex is $\mu = 1.5$.

Another essential dynamical test aims to simulate an experimentally relevant scenario of the creation of the HV mode. The most straightforward approach is to prepare two separate single-component condensates, with vorticities $+1$ and -1, and then load them into a common potential trap. In the optical realization of the model, the same scenario implies the coupling of two beams, carrying the opposite vorticities, into a common bulk waveguide. In either case, the modeling of this scenario means simulating Eqs. (2) with initial conditions which correspond to ψ_1 and ψ_2 taken as numerically exact solutions of the single-component equations, with $\beta = 0$ and vorticities ± 1. Figure 5 displays a typical example: In the course of the simulation, β was ramped from 0 to 0.2 during the time interval of $\Delta t = 20$. The simulations demonstrate (in this and other cases) that the initial vortex-antivortex mixture readily self-traps into the stationary HV state. Note that, although the example displayed in this figure, which pertains to $N = 5.65$ and the final value of $\beta = 0.2$, is located rather close to the instability border in Fig. 3, the evolution of the input mixture into the HV state does not excite any instability. We stress that this simulation was performed in the Cartesian coordinates, which would allow the onset of an axial-symmetry-breaking instability if the evolving mode was vulnerable to it.

C. The evolution of unstable HV states

It is also interesting to identify the outcome of the evolution of those HV modes which are unstable. Typical results are displayed in Figs. 6–8 for $\beta = 0.5$. This value of the interaction coefficient was chosen because the corresponding dominant instability modes feature three different values of the azimuthal index, *viz.*, $L = 1,2,3$, see Fig. 3. Accordingly, in Figs. 6, 7, and 8, we display the evolution of unstable HV states with $N = 7.5$, 13.5, and 8.75, that give rise to the leading unstable modes with $L = 1, 2$, and 3, respectively. We stress that, unlike the tests of the stable modes, no perturbations were added to

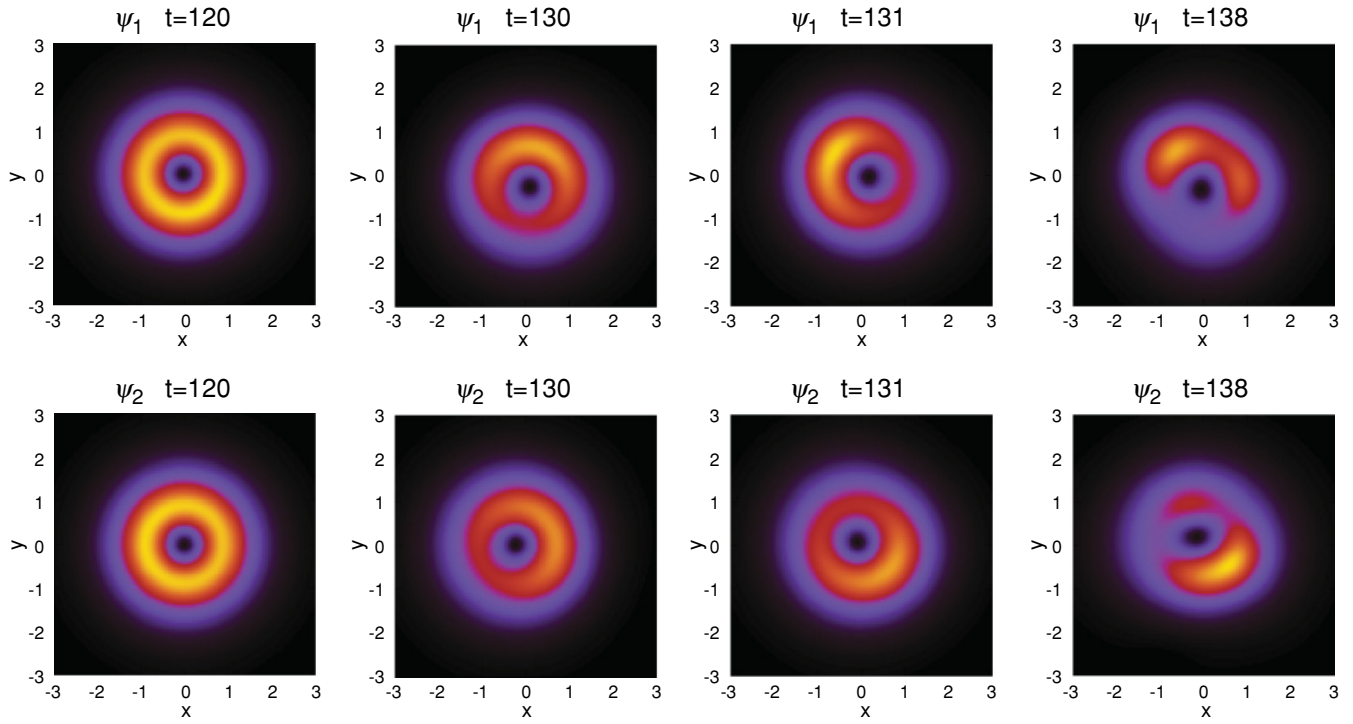

FIG. 6. (Color online) The evolution of the two components ψ_1 and ψ_2 of an unstable HV mode with half-norm $N = 7.5$ and $\mu = 0.83$. Density distributions are displayed at moments of time indicated above the respective panels. In this and two subsequent figures, $\beta = 0.5$ is fixed.

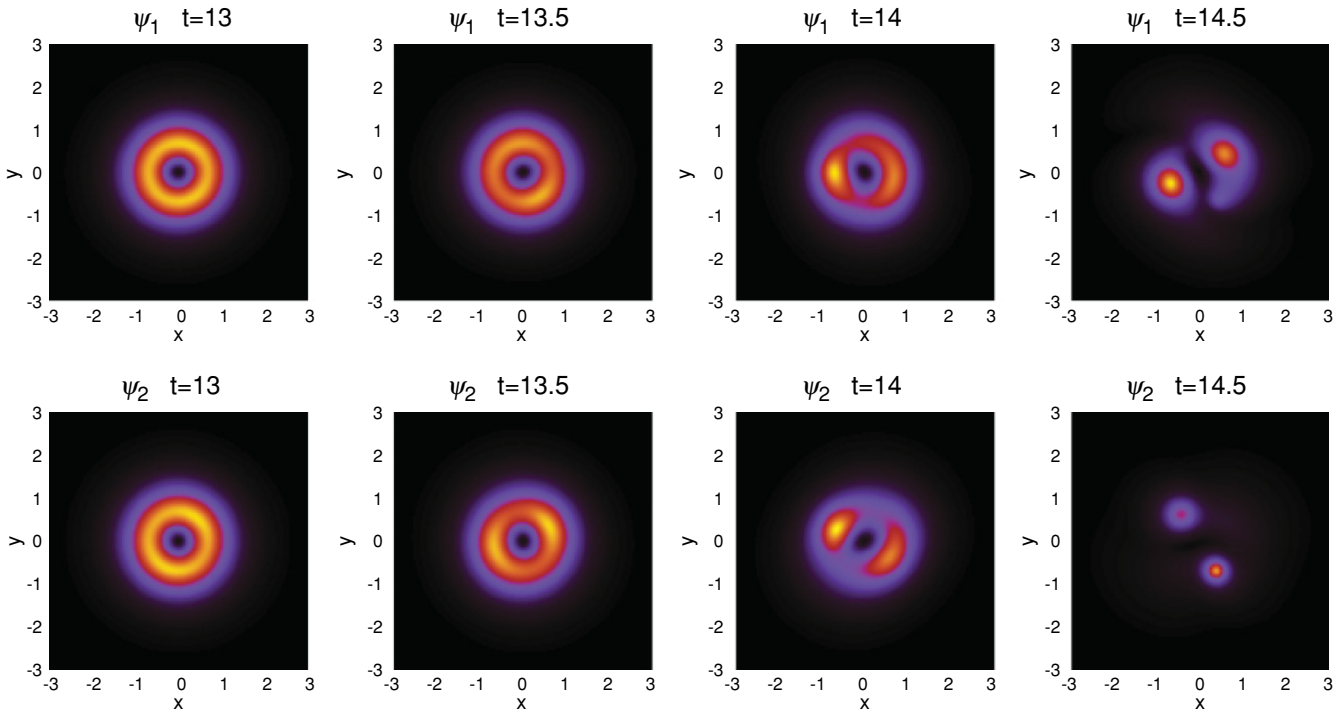

FIG. 7. (Color online) The same as in Fig. 6, but for $N = 13.49$, $\mu = -1.3$.

the unstable ones when simulating their evolution. The weak intrinsic noise generated by truncation errors of the numerical scheme was sufficient to invoke the instability.

The instability development driven by the eigenmode with $L = 1$, which is displayed in Fig. 6, is similar to that reported in Ref. [27], which studied the instability of two-component modes with the *explicit vorticity* (equal spins in the two components): The instability transforms the original axisymmetric mode into a deformed crescent-shaped pattern. Eventually, the pattern splits into two segments, which end up with the collapse. The splitting may be explained by the proximity to the instability mode corresponding to $L = 2$, see

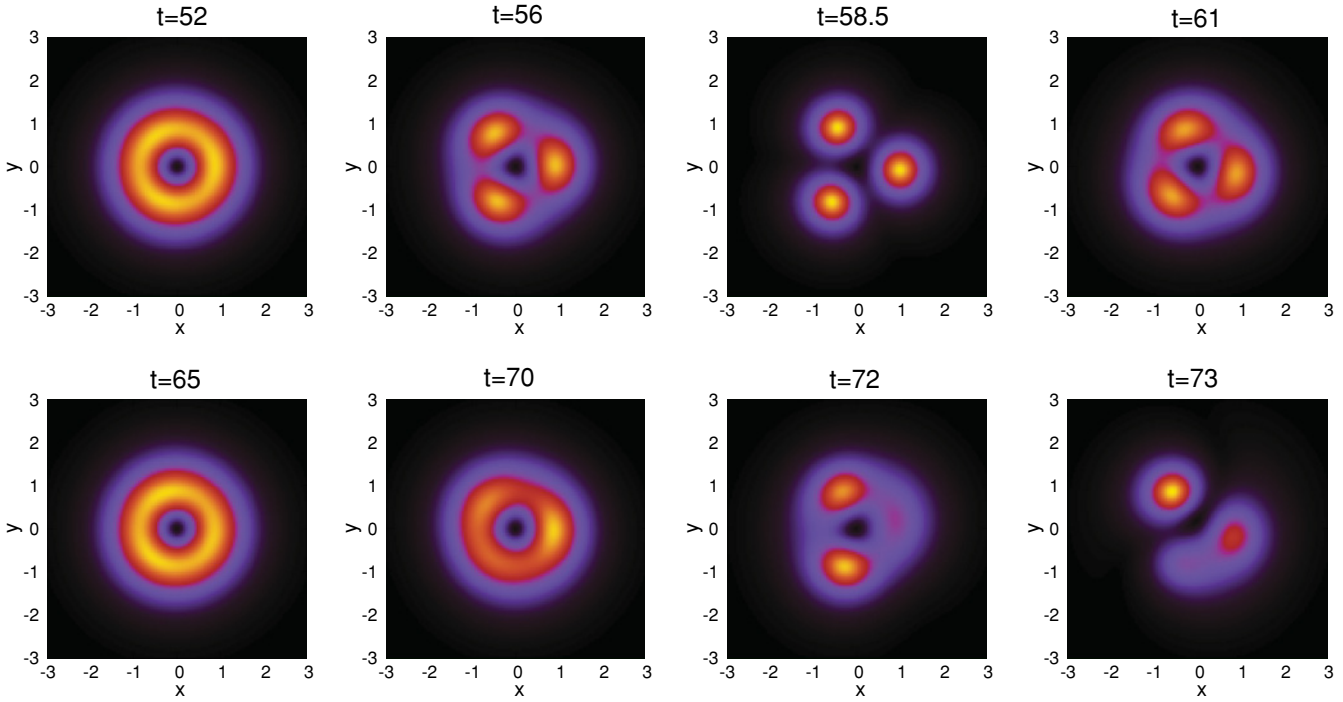

FIG. 8. (Color online) The evolution of an unstable HV state with $N = 8.75$, $\mu = 0.57$. In this case, the sequence of the density plots is shown only for ψ_1, the evolution of the second component being similar.

Fig. 3 (when the latter mode is the dominant one, it leads to the splitting, see Fig. 7).

In Fig. 7, the HV mode remains stable only up to $t \sim 13$—roughly, ten times as short as in Fig. 6, which may be readily explained by a much larger respective value of the instability growth rate, see Fig. 2. The eventual splitting of the unstable mode into two segments, which will collapse at a later stage of the evolution, is naturally explained by the azimuthal index of the dominant instability mode $L = 2$, similar to the instability of single- and two-component modes with the explicit vorticity [13,27].

The situation shown in Fig. 8 is somewhat different: The HV mode remains stable up to $t \simeq 52$. After that, it splits into three segments, in accordance with the fact that the linear instability is dominated by the mode with $L = 3$ in this case. The subsequent evolution leads to the temporary revival of the axisymmetric mode, around $t = 65$. It eventually becomes unstable at $t \simeq 73$, splitting into two, rather than three, segments (probably, this happens under the action of the second strongest unstable mode, with $L = 2$), which ultimately undergo the collapse. The trend for the temporary revival of the HV mode was observed in other cases too (for instance, at $N = 8.75$ and $\beta = 0.8$, although, in that case, the revival was incomplete).

We have checked that, in all cases, the (initial) splitting of unstable HV modes leads to the number of segments equal to the value of L, which corresponds to the most unstable perturbation eigenmode, provided that the initial norm is smaller than the above-mentioned collapse threshold $N_{\max}^{(S=1)}$ (if N exceeds this value, the mode directly proceeds to the collapse). In particular, the fast splitting into a set of four segments is observed too, as shown in Fig. 9, at $\beta = -0.5$, when the instability is dominated by the mode with $L = 4$, which has a large instability growth rate. It is also relevant to mention that the set of the splinters does not feature rotation, in accordance with the fact that the total angular moment of the original modes is zero.

IV. THE ANALYSIS OF THE 1D MODEL

The counterflow solutions to Eqs. (7), subject to BC (8), are

$$\psi_{1,2} = A \exp\left(\pm iS\frac{x}{\varrho} - i\mu t\right), \tag{12}$$

where S is the integer vorticity ($+S$ and $-S$ correspond to ψ_1 and ψ_2), μ is the chemical potential, and the amplitude is

$$A^2 = \left[\frac{1}{|\beta|} + \mathrm{sgn}\,(\beta)\right]^{-1}\left(\mu - \frac{S^2}{2\varrho^2}\right). \tag{13}$$

Solution (12) is the 1D counterpart of the HV mode, cf. Eq. (5).

The modulational instability of the CWs is analyzed by means of the standard approach [30], which takes the amplitude and phase of perturbed solutions as [cf. Eq. (10)]

$$a_{1,2}(x,t) = A + b_{1,2}\exp\left(-i\omega t + iL\frac{x}{\varrho}\right), \tag{14}$$

$$\Phi_{1,2}(x,t) = -\mu t \pm S\frac{x}{\varrho} + \chi_{1,2}\exp\left(-i\omega t + iL\frac{x}{\varrho}\right), \tag{15}$$

where $b_{1,2}$ and $\chi_{1,2}$ are amplitudes of small perturbations, $\mathrm{Im}\{\omega\}$ and L being the respective instability growth rate and azimuthal index. The substitution of these expressions into Eqs. (7), and the subsequent linearization yield, after simple algebraic manipulations, the following dispersion relations for ω:

$$\omega^2 = \frac{L^2}{\varrho^2}\left[S^2 + \frac{L^2}{4} - \frac{A^2\varrho^2}{|\beta|} \pm \sqrt{A^2\varrho^2\left(A^2\varrho^2 - \frac{4S^2}{|\beta|}\right) + S^2L^2}\right]. \tag{16}$$

A difference from the 2D model is that ω does not depend on the sign of the nonlinear coupling coefficient β.

The HV state is stable if expression (16) yields solely real values of ω (i.e., $\omega^2 > 0$). It is easy to see that this stability condition holds at

$$L^2 \geqslant L_{\max}^2 \equiv 4[S^2 + (1 + |\beta|^{-1})A^2\varrho^2]. \tag{17}$$

The commonly known possibility to suppress the modulational instability of zero-vorticity CWs, with $S = 0$, by means of the cyclic BC is to choose ϱ small enough, so as to make $L_{\max}^2 \leqslant 1$, hence all integers L will satisfy condition (17). However, in the case of HV states, with $S \geqslant 1$, this is obviously impossible. On the other hand, further consideration of Eq. (16) demonstrates that, in the case of $|\beta| \geqslant 2$, the *instability* region of L^2 may also be bounded from below:

$$4[S^2 - (1 - |\beta|^{-1})A^2\varrho^2] \equiv L_{\min}^2 < L^2 < L_{\max}^2, \tag{18}$$

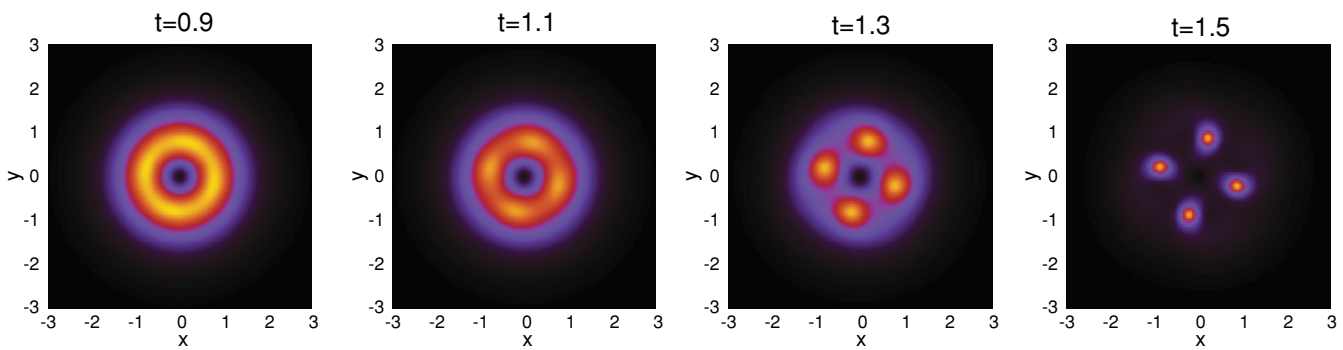

FIG. 9. (Color online) The same as in Fig. 8, but for $\beta = -0.5$ and $N = 34.1$, $\mu = -0.2$. In this case, the HV state quickly splits into a set of four segments.

where $L_{\max}$ is the same as in Eq. (17), and an additional condition is $L_{\min}^2 > 0$ (a similar situation occurs in the study of the modulational instability in the system of *XPM*-coupled nonlinear Schrödinger equations in fiber optics, with the self-defocusing nonlinearity and $\beta = -2$, the role of the HV (opposite momenta in the two components), being is played by the group-velocity mismatch between the two waves [30]). Thus, another stabilization mechanism for the HV state might be possible if no integer L would get into interval (18) for given $S \geqslant 1$. However, an explicit analysis of the latter condition leads, eventually, to inequality $L < 2S < L + 1$, which must hold for some integer $L \geqslant 1$, but, obviously, it can never hold [the meaning of this inequality is the existence of a stability window *between* instability regions (18) for L and $L + 1$]. Thus, the HV states in the simple 1D model (7) can never be stable, contrary to their HV counterparts in the 2D system (2).

V. CONCLUSION

In this paper, we have investigated a family of 2D nonlinear trapped modes in the form of the symmetric bound state of two components with opposite vorticities $S_{1,2} = \pm 1$, in the system with attractive cubic interactions, which act inside the components, while the interaction between the components may be either attractive or repulsive. Although the shape of the unperturbed modes is the same as in previously investigated states with explicit vorticity ($S_1 = S_2 = 1$), the stability of the presently considered HV modes is a novel problem. The stability region for the HV state has been identified through the calculation of the stability eigenvalues for small perturbations and verified against direct simulations with large random perturbations added to the HV mode. The stability domain is the main result of this paper (*a priori*, it was not obvious if HV modes might be stable at all; indeed, analyzing the simplified 1D model, based on the system of coupled equations with the cyclic BC, we have found that the 1D system can never give rise to stable HV modes). As could be expected, when the 2D HV modes are unstable, in direct simulations, they split into sets of fragments whose number is equal to the azimuthal index (L) of the most unstable perturbation eigenmode. If the instability is weak, which corresponds to $L = 3$, the splitting HV mode is temporarily recovered before the final splitting.

The 2D model directly applies to the description of the trapped binary BEC and may also describe the propagation of bimodal beams of light in photonic-crystal fibers. The simplified 1D system models the binary BEC in a toroidal trap, where the HV state corresponds to the counterflows in the two components and the propagation of a bimodal optical beam in a hollow cylindrical waveguide.

In the experiment, the 2D HV state in the optical system can easily be created by coupling the two beams with opposite vorticities into the same bulk waveguide. In the BEC, it may be difficult to directly impart opposite vorticities to two components, which represent different states of the same atomic species. However, another scenario may be realized: At first, two states with the opposite vorticities can be prepared separately, and then loaded into the same trap, as illustrated previously by Fig. 5.

A challenging problem for the extension of the present analysis is to consider 3D bimodal solitons with the HV. It may also be interesting to consider two-component vortical gap solitons of the HV type, supported by an optical lattice in the 2D system with the repulsive nonlinearity.

ACKNOWLEDGMENTS

M.B. and A.G. thank FAPESP/CNPq (Brazil) for financial support. The work of B.A.M. was supported, in part, by the German-Israel Foundation through Grant No. 149/2006.

[1] M. R. Matthews, B. P. Anderson, P. C. Haljan, D. S. Hall, C. E. Wieman, and E. A. Cornell, Phys. Rev. Lett. **83**, 2498 (1999); A. E. Leanhardt, A. Görlitz, A. P. Chikkatur, D. Kielpinski, Y. Shin, D. E. Pritchard, and W. Ketterle, *ibid.* **89**, 190403 (2002); P. Engels, I. Coddington, V. Schweikhard, and E. A. Cornell, J. Low Temp. Phys. **134**, 683 (2004); A. L. Fetter, Rev. Mod. Phys. **81**, 647 (2009).

[2] G. A. Swartzlander Jr. and C. T. Law, Phys. Rev. Lett. **69**, 2503 (1992); A. W. Snyder, L. Poladian, and D. J. Mitchell, Opt. Lett. **17**, 789 (1992).

[3] B. A. Malomed, D. Mihalache, F. Wise, and L. Torner, J. Opt. B **7**, R53 (2005).

[4] A. Görlitz *et al.*, Phys. Rev. Lett. **87**, 130402 (2001).

[5] V. I. Kruglov, V. M. Volkov, R. A. Vlasov, and V. V. Drits, J. Phys. A **21**, 4381 (1988); V. I. Kruglov, Yu. A. Logvin, and V. M. Volkov, J. Mod. Opt. **39**, 2277 (1992).

[6] W. J. Firth and D. V. Skryabin, Phys. Rev. Lett. **79**, 2450 (1997); L. Torner and D. V. Petrov, Electron. Lett. **33**, 608 (1997); D. Mihalache, D. Mazilu, L.-C. Crasovan, B. A. Malomed, and F. Lederer, Phys. Rev. E **61**, 7142 (2000).

[7] M. Quiroga-Teixeiro and H. Michinel, J. Opt. Soc. Am. B **14**, 2004 (1997); I. Towers, A. V. Buryak, R. A. Sammut, and B. A. Malomed, Phys. Rev. E **63**, 055601(R) (2001); B. A. Malomed, L.-C. Crasovan, and D. Mihalache, Physica D **161**, 187 (2002); D. Mihalache, D. Mazilu, L.-C. Crasovan, I. Towers, A. V. Buryak, B. A. Malomed, L. Torner, J. P. Torres, and F. Lederer, Phys. Rev. Lett. **88**, 073902 (2002); T. A. Davydova and A. I. Yakimenko, J. Opt. A: Pure Appl. Opt. **6**, S197 (2004); D. Mihalache, D. Mazilu, B. A. Malomed, and F. Lederer, Phys. Rev. E **69**, 066614 (2004); H. Michinel, J. R. Salgueiro, and M. J. Paz-Alonso, *ibid.* **70**, 066605 (2004).

[8] D. Briedis, D. E. Petersen, D. Edmundson, W. Królikowski, and O. Bang, Opt. Express **13**, 435 (2005); A. I. Yakimenko, Y. A. Zaliznyak, and Y. Kivshar, Phys. Rev. E **71**, 065603 (2005).

[9] I. Tikhonenkov, B. A. Malomed, and A. Vardi, Phys. Rev. A **78**, 043614 (2008).

[10] B. B. Baizakov, B. A. Malomed, and M. Salerno, Europhys. Lett. **63**, 642 (2003); J. Yang and Z. H. Musslimani, Opt. Lett. **28**, 2094 (2003).

[11] Y. V. Kartashov, V. A. Vysloukh, and L. Torner, Phys. Rev. Lett. **94**, 043902 (2005); Y. V. Kartashov, R. Carretero-González, B. A. Malomed, V. A. Vysloukh, and L. Torner, Opt. Express **13**, 10703 (2005).

[12] F. Dalfovo and S. Stringari, Phys. Rev. A **53**, 2477 (1996); R. J. Dodd, J. Res. Natl. Inst. Stand. Technol. **101**, 545 (1996); T. J. Alexander and L. Bergé, Phys. Rev. E **65**, 026611 (2002); L. D. Carr and C. W. Clark, Phys. Rev. Lett. **100**, 019903(E) (2008).

[13] D. Mihalache, D. Mazilu, B. A. Malomed, and F. Lederer, Phys. Rev. A **73**, 043615 (2006); B. A. Malomed, F. Lederer, D. Mazilu, and D. Mihalache, Phys. Lett. A **361**, 336 (2007).

[14] L. Bergé, Phys. Rep. **303**, 259 (1998).

[15] A. S. Desyatnikov and Y. S. Kivshar, Phys. Rev. Lett. **87**, 033901 (2001); M. S. Bigelow, Q.-H. Park, and R. W. Boyd, Phys. Rev. E **66**, 046631 (2002); F. Ye, J. Wang, L. Dong, and Y. P. Li, Opt. Commun. **230**, 219 (2004).

[16] A. S. Desyatnikov, D. Mihalache, D. Mazilu, B. A. Malomed, C. Denz, and F. Lederer, Phys. Lett. A **364**, 231 (2007).

[17] A. V. Mamaev, M. Saffman, and A. A. Zozulya, J. Opt. B **6**, S318 (2004).

[18] A. S. Desyatnikov, D. Mihalache, D. Mazilu, B. A. Malomed, C. Denz, and F. Lederer, Phys. Rev. E **71**, 026615 (2005).

[19] J. P. Torres, J. M. Soto-Crespo, L. Torner, and D. V. Petrov, Opt. Commun. **149**, 77 (1998); H. Leblond, B. A. Malomed, and D. Mihalache, Phys. Rev. E **71**, 036608 (2005).

[20] P. G. Kevrekidis and D. E. Pelinovsky, Proc. R. Soc. London, Ser. A **462**, 2671 (2006).

[21] L. Pitaevskii and S. Stringari, *Bose-Einstein Condensation* (Clarendon Press, Oxford, 2003).

[22] S. B. Papp, J. M. Pino, and C. E. Wieman, Phys. Rev. Lett. **101**, 040402 (2008); P. Zhang, P. Naidon, and M. Ueda, *ibid.* **103**, 133202 (2009).

[23] S. Gupta, K. W. Murch, K. L. Moore, T. P. Purdy, and D. M. Stamper-Kurn, Phys. Rev. Lett. **95**, 143201 (2005); C. Ryu, M. F. Andersen, P. Cladé, V. Natarajan, K. Helmerson, and W. D. Phillips, *ibid.* **99**, 260401 (2007); J. Smyrnakis, M. Magiropoulos, G. M. Kavoulakis, and A. D. Jackson, Phys. Rev. A **81**, 063601 (2010).

[24] L. Wen, H. Xiong, and B. Wu, e-print arXiv:1003.2798v2.

[25] M. Tsubota, K. Kasamatsu, and M. Ueda, Phys. Rev. A **65**, 023603 (2002); K. Kasamatsu, M. Tsubota, and M. Ueda, *ibid.* **67**, 033610 (2003).

[26] T. M. Monro and D. J. Richardson, C. R. Phys. **4**, 175 (2003); S. Arismar Cerqueira Jr., Rep. Prog. Phys. **73**, 024401 (2010).

[27] A. I. Yakimenko, Y. A. Zaliznyak, and V. M. Lashkin, Phys. Rev. A **79**, 043629 (2009).

[28] M. Brtka, A. Gammal, and L. Tomio, Phys. Lett. A **359**, 339 (2006).

[29] Y. G. D'yakonov, Zh. Vych. Mat. **2**, 549 (1962) [USSR Comput. Math. Math. Phys. **2**, 581 (1963)]; see also D. Quinney, *An Introduction to the Numerical Solution of Differential Equations*, revised ed. (Res. Stud. Press/Wiley, New York, 1987).

[30] G. P. Agrawal, Phys. Rev. Lett. **59**, 880 (1987).